# Source clustering effects on the skewness of the lensing convergence

Takashi Hamana<sup>1</sup>, Stéphane T. Colombi<sup>1,2</sup>, Aurélien Thion<sup>1</sup>, Julien E. G. T. Devriendt<sup>3</sup>, Yannick Mellier<sup>1,4</sup> and Francis Bernardeau<sup>5</sup>

- <sup>1</sup> Institut d'Astrophysique de Paris, CNRS, 98bis Boulevard Arago, F75014 PARIS, France
- <sup>2</sup>NIC (Numerical Investigations in Cosmology) Group, CNRS
- <sup>3</sup> Nuclear & Astrophysics Laboratory, University of Oxford, Keble road, OX1 3RH Oxford UK
- <sup>4</sup> Observatoire de Paris, DEMIRM, 61 avenue de l'Observatoire, 75014 PARIS, France
- <sup>5</sup>Service de Physique Théorique, C.E. de Saclay, 91191 Gif sur Yvette Cedex, France

Accepted ....; Received ....; in original form ....

#### ABSTRACT

The correlation between source galaxies and lensing potentials causes systematic effect on measurements of cosmic shear statistics, the so-called source clustering (SC) effect. The SC effect on the skewness of lensing convergence,  $S_3$ , is examined using a nonlinear semi-analytic approach and is checked against numerical simulations. The semi-analytic calculations have been performed in a wide variety of generic models for the redshift distribution of source galaxies and power-law models for the bias parameter between galaxy and dark matter distribution. A very good agreement is found between semi-analytic predictions and numerical simulations. We find the relative amplitude of SC effect on  $S_3$  to be of the order of 5-40%. It depends significantly on the redshift distribution of sources and on the way the bias parameter evolves. We discuss possible measurement strategies to that would minimize the SC effects.

**Key words:** cosmology: theory — dark matter — gravitational lensing — large-scale structure of universe

# 1 INTRODUCTION

Recent detections of the cosmic shear signal have opened a new window to probe the distribution of matter in the universe, its evolution, and to test cosmological models (Van Waerbeke et al. 2000a; Wittman et al. 2000; Bacon, Refregier & Ellis 2000; Kaiser, Wilson & Luppino 2000; Maoli et al 2000). These detections were obtained from relatively small fields so far, which limit the statistical analyses of the surveys to second order moments, the variance or two-point correlation function of cosmic shear. The amplitude of second order statistics reflects that of density fluctuations and roughly scales as  $\sigma_{\gamma} \propto \Omega_{\rm m}^{0.6-0.8} \sigma_8$  at large scale (Bernardeau, Van Waerbeke & Mellier 1997, hereafter BvWM97) and  $\sigma_{\gamma}\,\propto\,\Omega_{\rm m}^{0.6-0.8}\sigma_{8}^{1.2-1.3}$ at small scale (Jain & Seljak 1997, Maoli et al. 2000). On the other hand, the skewness of lensing convergence is known to be sensitive to  $\Omega_{\rm m}$  almost independently on  $\sigma_8$  (BvWM97). Therefore, combined analysis of the skewness and the variance will provide precious constraints on both values of  $\Omega_{\rm m}$  and  $\sigma_8$ . As a consequence, skewness detection and measurement is one of main goals of on-going wide field cosmic shear surveys such as the DESCART project  $\!\!\!^\star$  .

Cosmic shear statistics have been studied analytically (see Mellier 1999 and Bartelmann & Schneider 2000 for reviews and references therein) as well as numerically (Jain, Seljak & White 2000; White & Hu 2000). The skewness of lensing convergence was first calculated by BvWM97 based on quasi-linear perturbation theory approach. It has been, however, recognized that this approach is not robust enough to provide accurate predictions for the values of the skewness in all available dynamic range. In particular, the two following points have to be addressed and carefully included in the calculations: (i) Nonlinear growth of the density field: numerical studies showed that nonlinear growth enhances skewness especially at angular scales smaller than 10 arcmin (Jain et al. 2000; White & Hu 2000, Van Waerbeke et al. 2000b). (ii) Source clustering: Bernardeau (1998) (hereafter B98) pointed out that correlations between source galaxies and lensing potential reduce skewness amplitude.

<sup>\*</sup> For more information about DESCART project, see http://terapix.iap.fr/Descart/

B98 underlined that this effect is sensitive to the redshift distribution of sources.

The purpose of this paper is to examine the effect of source clustering (SC) on measurements of the skewness of lensing convergence. Special attention is payed to its dependence on the redshift distribution of sources and on evolution of bias between matter and galaxy distribution. Since redshift distribution of faint galaxies is uncertain and little is known about the bias, this paper does not aim at making accurate predictions for the amplitude of SC effect in real cosmic shear surveys. Our objective is to estimate its magnitude in order to propose strategies that minimize its effects.

We basically follow the perturbation theory approach first developed by B98 but generalize it in two ways: (i) we take into account the effects of nonlinear evolution of the density field, adopting the nonlinear semi-analytic ansatz developed by Jain & Seljak (1997) and Van Waerbeke et al. (2000b); (ii) we allow a possible redshift dependence of the bias parameter,  $b(z) = b_0(1+z)^{\gamma}$  and examine the cases  $\gamma = 0$  to 2. Moreover we consider three cosmological Cold Dark Matter family models (CDM), two flat models with and without cosmological constant and an open model, and 12 different models for the source distribution which cover a wide range of mean redshift and width for the distribution.

Finally for the first time the accuracy of semi-analytic predictions for the SC effects on the skewness is tested against numerical simulations in standard CDM model.

The outline of this paper is as follows. In section 2, physical mechanism of SC is described. In section 3, expression for the skewness of lensing convergence is presented while taking both SC and nonlinear evolution of the density field into account. In section 4, our models are described. Results of the semi-analytic approach are presented in section 5. In section 6, semi-analytic predictions are tested against numerical simulations and discussed in section 7.

## 2 WHAT IS THE SC EFFECT?

The SC effect discussed in this paper comes into light because of the conjunction of three circumstances, namely: (i) source galaxies are not randomly distributed in the sky but are correlated; (ii) the source galaxy distribution traces somehow the matter field; (iii) the redshift distribution of source galaxies is rather broad. Its width depends on source selection criterion. Consequently, the distribution of source galaxies overlaps with the distribution of lensing structures, and thus source galaxies are somehow correlated with lensing potential. This correlation causes systematic effects on measurements of cosmic shear, that may be illustrated as follows. Figure 1 shows, for example, the distribution of sources (denoted by filled circles) and the gravitational potential (contour lines). For a line-of-sight 1 (LOS 1), the distant galaxies are lensed by the gravitational potential located at intermediate distance and thus have a high positive lensing signal. This high signal is reduced by the excess of foreground sources bound to the foreground gravitational potential which, in contrast, have a low lensing signal. On the other hand, for a line-of-sight 2 (LOS 2), distant sources are lensed by the foreground void and thus have a negative lensing signal. This negative signal is amplified because

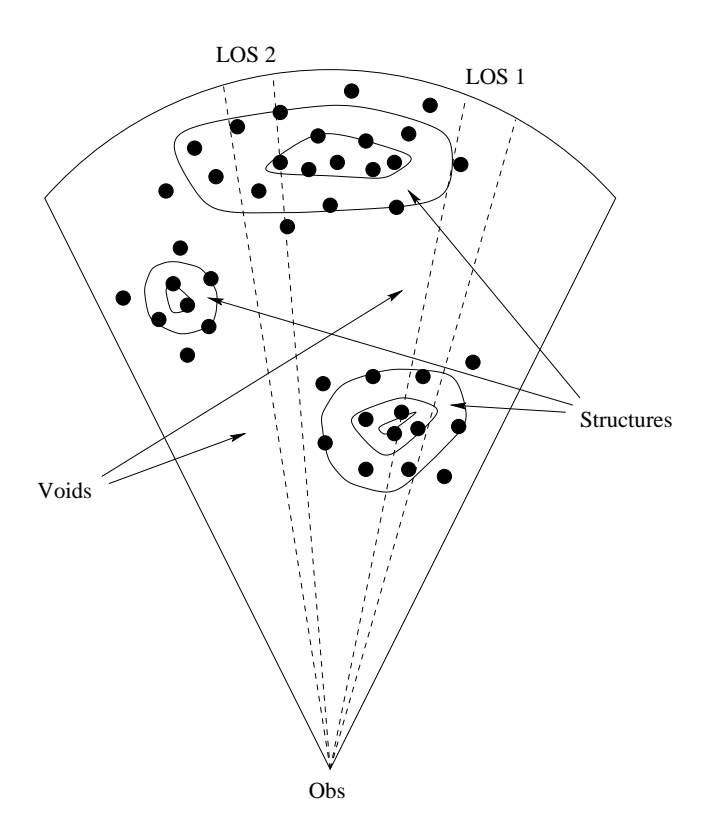


**Figure 1.** An illustration of the correlation between the gravitational potential (contour lines) and the population of sources (denoted by filled circles).

of the lack of foreground sources in the void. Accordingly, the probability distribution function of the lensing signal, i.e. the lensing convergence, becomes more symmetric than for the case of a random distribution of source galaxies. As a result, the amplitude of skewness of lensing convergence drops.

As was pointed out by B98, there is another possible effect caused by intrinsic clustering of source galaxies. The average distance of sources may indeed vary from one direction to another, which may cause systematic effects on the cosmic shear statistics. It was pointed out by B98 that this effect can, in general, be neglected. Therefore, in this analysis, we do not take it into account for the analytical calculations presented in next section, although it will be obviously present in the numerical experiments discussed in § 6.

# 3 THE PERTURBATION THEORY APPROACH

# 3.1 The quasi-linear regime

The expression for the skewness of lensing convergence was first derived by BvWM97 and the correction term due to SC was derived by B98 in the framework of perturbation theory. In this subsection, we only focus on expressions which are directly relevant to this paper. We refer the reader to BvWM97 and B98 for details.

In the linear regime, the variance of the top-hat filtered lensing convergence is related to the linear density power spectrum through

$$V_{\kappa}(\theta) \equiv \langle \kappa^{2}(\theta) \rangle$$

$$= \frac{1}{2\pi} \left(\frac{H_{0}}{c}\right)^{2} \int_{0}^{\chi_{\text{max}}} d\chi_{l} w^{2}(\chi_{l}) I_{0}(\chi_{l}, \theta), \qquad (1)$$

with

$$I_0(\chi,\theta) = \int dk \, k P_{\text{lin}}(\chi,k) W_{\text{2D}}^2[kf(\chi)\theta] \,. \tag{2}$$

In these equations,  $\chi$  is the comoving radial distance,  $\chi_{\rm max}$  is determined by the redshift of the most distant source galaxy,  $P_{\rm lin}[\chi(a),k]$  is the linear density power spectrum and a is the scale factor of the Universe normalized by its present value  $[a(t=t_0)=1]$ . Function  $f(\chi)$  is the corresponding comoving angular diameter distance, defined as  $f(\chi)=K^{-1/2}\sin K^{1/2}\chi$ ,  $\chi$ ,  $(-K)^{-1/2}\sinh (-K)^{1/2}\chi$  for K>0, K=0, K<0, respectively, where K is the curvature which can be expressed in function of the matter density parameter  $\Omega_{\rm m}$  and the cosmological constant parameter  $\Omega_{\lambda}$  as  $K=(H_0/c)^2(\Omega_{\rm m}+\Omega_{\lambda}-1)$ . Finally, function  $W_{\rm 2D}(x)$  is the Fourier transform of the angular top-hat filter given by  $W_{\rm 2D}(x)=2J_1(x)/x$ , where  $J_1$  is the spherical Bessel function of first kind.

The lensing efficiency function,  $w(\chi)$ , is defined by,

$$w(\chi_l) = \frac{3\Omega_{\rm m}}{2} \frac{H_0}{c} \frac{f(\chi_l)}{a(\chi_l)} \int_{\chi_l}^{\chi_{\rm max}} d\chi_s \frac{f(\chi_s - \chi_l)}{f(\chi_s)} \frac{dn_s(\chi_s)}{d\chi_s} , \quad (3)$$

where  $n_s[\chi(z)]$  is the redshift distribution of source galaxies and  $\chi_l$  and  $\chi_s$  denote the radial distance to the lens and the source, respectively.

Following B98, we assume that the number density of sources can be expressed as  $n_s(\chi,\theta_1,\theta_2)=n_s(\chi)\left(1+\delta_s\left(\chi,\theta_1,\theta_2\right)\right)$ , and linear biasing, i.e.,  $\delta_s(\chi,\theta_1,\theta_2)=b(\chi)\delta_{\rm mass}(\chi,\theta_1,\theta_2)$ , Generalizing equation (29) of B98 for an arbitrary Friedmann model and a general form of the density power spectrum, the expression of skewness parameter,  $S_3=\langle\kappa^3(\theta)\rangle/\langle\kappa^2(\theta)\rangle^2$ , is given by the quasi-linear term,  $S_3^{q,l}$ , and a correction term due to SC,  $S_3^{q,l}$ .

$$S_3(\theta) = S_3^{q.l.}(\theta) + S_3^{s.c.}(\theta),$$
 (4)

with

$$S_3^{q.l.}(\theta) = \frac{1}{V_\kappa^2(\theta)} \frac{6}{(2\pi)^2} \left(\frac{H_0}{c}\right)^3 \int_0^{\chi_{\text{max}}} d\chi \, w^3(\chi) \\ \times \left[\frac{6}{7} I_0^2(\chi, \theta) + \frac{1}{2} I_0(\chi, \theta) I_1(\chi, \theta)\right], \tag{5}$$

$$S_3^{s.c.}(\theta) = \frac{1}{V_\kappa^2(\theta)} \frac{9\Omega_{\rm m}}{(2\pi)^2} \left(\frac{H_0}{c}\right)^4 \times \int_0^{\chi_{\rm max}} d\chi \, w(\chi) \frac{dn_s(\chi)}{d\chi} b(\chi) I_0(\chi, \theta) \frac{1}{f(\chi)} \times \int_0^{\chi} d\chi' \, w(\chi') f(\chi - \chi') f(\chi') \frac{1}{a(\chi')} I_0(\chi', \theta) - \frac{1}{V_\kappa(\theta)} \frac{3}{\pi} \frac{H_0}{c} \int_0^{\chi_{\rm max}} d\chi \, w(\chi) \frac{dn_s(\chi)}{d\chi} \times b(\chi) I_0(\chi, \theta),$$

$$(6)$$

where

$$I_1(\chi,\theta) = \int dk \, k^2 P_{\text{lin}}(\chi,k) W_{\text{2D}}[kf(\chi)\theta] \frac{dW_{\text{2D}}[kf(\chi)\theta]}{dk} \,. \quad (7)$$

In deriving the above expressions, we have assumed that averaging of shapes over source galaxies is done with angular top-hat filter. Moreover, we have taken the continuous limit for the source distribution (B98). Note that other source clustering effects can appear because of discreteness effects as such those described by Thion et al. (2000).

#### 3.2 Nonlinear regime

For the variance of the lensing convergence, effect of nonlinear evolution of the density power spectrum can be included by replacing the linear power spectrum with the nonlinear power spectrum, i.e.,  $P_{\rm lin}(a,k) \to P_{\rm NL}(a,k)$  (Jain & Seljak 1997). We use the fitting formula of nonlinear power spectrum given by Peacock and Dodds (1996). This semi-analytic approach has been tested against ray-tracing simulations, and a good agreement between the numerical results and the semi-analytic predictions was found (Jain et al 2000, White and Hu 2000).

In the framework of perturbation theory, all density contrasts needed for the calculation of the skewness correction term, equation (6), correspond to linear order (see B98 for details). This is the same situation as for the variance. Following the procedure used for this latter case, we simply replace the linear power spectrum with the nonlinear one to include nonlinear effects.

The semi-analytic calculation of the skewness in the nonlinear regime was developed by Van Waerbeke et al. (2000b). It is based on the fitting formula of the density bispectrum by Scoccimarro & Couchman (2000) and is given by

$$S_3^{n.l.}(\theta) = \frac{1}{V_\kappa^2(\theta)} \frac{6}{(2\pi)^4} \left(\frac{H_0}{c}\right)^3 \int_0^{\chi_{\text{max}}} d\chi \, w^3(\chi) D_+^3(\chi)$$

$$\times \int d^2 \mathbf{k_1} \, P_0(k_1) W_{2D}[k_1 f(\chi) \theta]$$

$$\times \int d^2 \mathbf{k_2} \, P_0(k_2) W_{2D}[k_2 f(\chi) \theta]$$

$$\times W_{2D}[|\mathbf{k_1} + \mathbf{k_2}| f(\chi) \theta] F_2^{\text{eff}}(\mathbf{k_1}, \mathbf{k_2}), \qquad (8)$$

where

$$F_2^{\text{eff}}(\mathbf{k_1}, \mathbf{k_2}) = \frac{5}{7} a(n, k_1) a(n, k_2) + \frac{1}{2} b(n, k_1) b(n, k_2) \frac{\mathbf{k_1} \cdot \mathbf{k_2}}{k_1 k_2} \left( \frac{k_1}{k_2} + \frac{k_2}{k_1} \right) + \frac{2}{7} c(n, k_1) c(n, k_2) \frac{(\mathbf{k_1} \cdot \mathbf{k_2})^2}{|k_1|^2 |k_2|^2}.$$
(9)

Here  $D_+(\chi)$  is the linear growth factor (Peebles 1980) normalized to its present value and  $P_0(k)$  is the linear density power spectrum at present time. Functions a(n,k), b(n,k) and c(n,k) depend on the effective power spectral index n at scale k (explicit expressions are given in Scoccimarro & Couchman 2000; see also Van Waerbeke et al. 2000b). It should be noted that, since the bispectrum fitting formula is constructed via the dark matter bispectrum measured from only one N-body simulation data set, there is about a 10-20 percent uncertainty in the fitting formula. This is mainly a cosmic variance effect (Van Waerbeke et al. 2000b).

Table 1. Cosmological parameters.

Model	$\Omega_{\mathrm{m}}$	$\Omega_{\lambda}$	h	$\sigma_8$
SCDM	1.0	0.0	0.5	0.6
OCDM	0.3	0.0	0.7	0.85
$\Lambda \mathrm{CDM}$	0.3	0.7	0.7	0.9

**Table 2.** Parameters in  $n_s(z)$ .

Model	$\langle z \rangle$	$\Delta z$	$\alpha$	β	$z_*$
A1	1.2	0.572	2	1.5	0.798
A2	1.2	0.456	3	1.8	0.813
A3	1.2	0.297	5	3.0	1.01
A4	1.2	0.182	8	6.0	1.18
B1	1.5	0.866	2	1.0	0.500
B2	1.5	0.618	3	1.5	0.812
B3	1.5	0.400	5	2.5	1.11
B4	1.5	0.244	7	6.0	1.51
C1	0.9	0.429	2	1.5	0.598
C2	0.9	0.342	3	1.8	0.610
C3	0.9	0.240	5	2.5	0.667
C4	0.9	0.136	8	6.0	0.884

# 4 MODELS

#### 4.1 Cold dark matter models (CDM)

We discuss three Cold Dark Matter (CDM) models, a flat model with ( $\Lambda$ CDM) and without cosmological constant (SCDM) and an open model (OCDM), using galaxy cluster abundances to normalize the power-spectrum (Eke, Cole & Frenk, 1996; Kitayama & Suto 1997) and the formula of Bond & Efstathiou (1984) for the transfer function. The parameters in the models are listed in Table 1.

#### 4.2 Redshift distribution of source galaxies

We assume that  $n_s(z)$  takes the form,

$$\frac{dn_s(z)}{dz} = \frac{\beta}{z_* \Gamma[(1+\alpha)/\beta]} \left(\frac{z}{z_*}\right)^{\alpha} \exp\left[-\left(\frac{z}{z_*}\right)^{\beta}\right]. \tag{10}$$

where  $\Gamma(x)$  is the Gamma function.

We explore 12 models for the shape of the distribution. The parameters in each model are listed in Table 2. The average redshift is  $\langle z \rangle = 1.2, 1.5$  and 0.9 for models A1-4, B1-4 and C1-4, respectively. We characterize the width of the distribution by the root-mean-square,  $\Delta z$ , which varies within a factor of  $\simeq 3.2, 3.5$  and 3.2 in models A1-4, B1-4 and C1-4, respectively. Note that only model A1 matches roughly the observed redshift distribution of galaxies in current cosmic shear detections (Van Waerbeke et al. 2000a). However, to keep our approach as general as possible, we still use a reasonably large parameter range for the possible shapes of the distributions.

Figure 2 shows the redshift distribution of sources and the corresponding lensing efficiency function as functions of redshift. In top panel, SCDM is supposed, and various models for galaxy number counts are taken. In bottom panel,

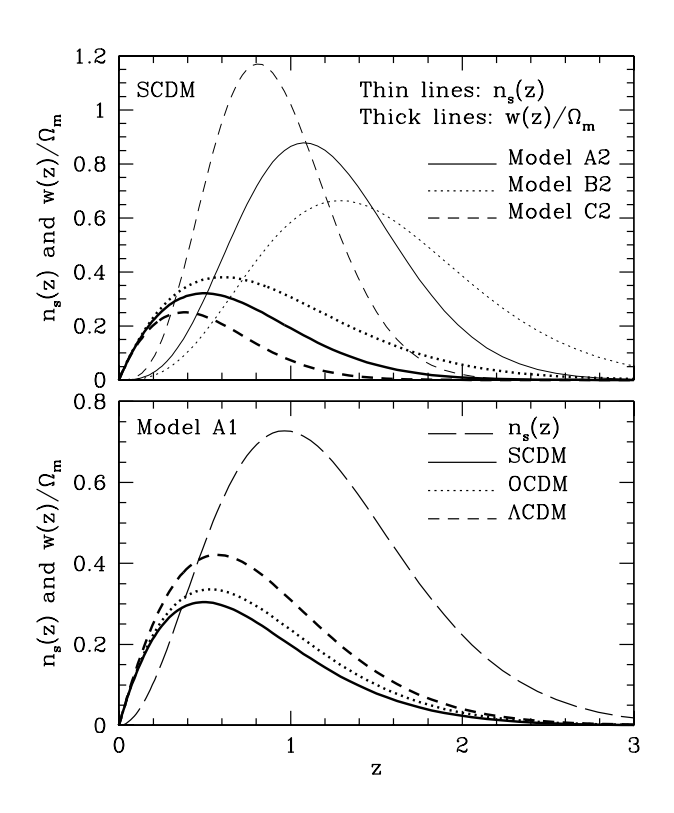


Figure 2. The redshift distributions of sources,  $n_s(z)$ , and the corresponding lensing efficiency functions divided by the density parameter,  $w(z)/\Omega_{\rm m}$ , as functions of redshift. Top panel: for three source distribution models in SCDM model. Bottom panel: for A1 model in three cosmologies.

model A1 is assumed for number counts, and various cosmologies are considered. Roughly speaking, the amplitude of SC is controlled by the amplitude of overlapping between the population of sources  $[n_s(z)]$  and that of lenses [which is very closely related to  $w(z)/\Omega_{\rm m}$ ]. It is important to keep in mind that the normalized efficiency function  $w(z)/\Omega_{\rm m}$  increases in order of SCDM, OCDM and  $\Lambda$ CDM.

#### 4.3 Model for the bias

We assume that the bias between the galaxy and the matter distribution is linear and takes a power-law form as a function of redshift, i.e.,

$$b(z) = b_0 (1+z)^{\gamma}. \tag{11}$$

We examine three cases,  $\gamma = 0$ , 1 and 2, and we shall take  $b_0 = 1$ . Since, so far, little is known about a realistic description of the bias, we adopted this model for its simplicity and the wide possible range of possibilities it nevertheless covers. Numerical studies of dark matter clustering combined with measurements of two-point correlation function in galaxy catalogs suggested that  $b_0$  is close to unity (e.g., Jenkins et al. 1998).

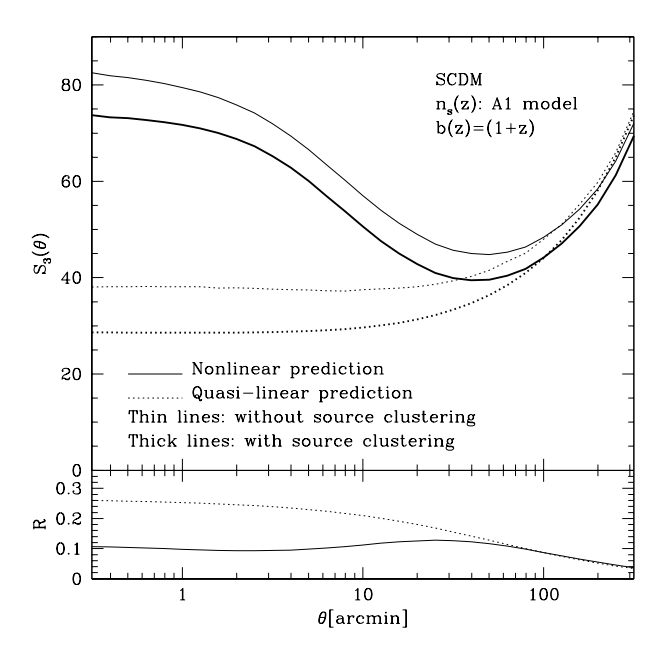


Figure 3. Upper panel: predicted skewness of the lensing convergence for A1 and SCDM, with and without source clustering effect taken into account. Lower panel: the ration R as defined in equation (12).

#### 5 RESULTS

Let us introduce the parameter which characterizes the amplitude of the SC effects defined by

$$R = -\frac{S_3^{s.c.}}{S_3},\tag{12}$$

where  $S_3^{s.c.}$  is the correction brought by SC and  $S_3$  is the true skewness (without SC).

Figure 3 shows  $S_3$  with and without taking the SC effect into account as a function of  $\theta$  (upper panel) and R (lower panel) for A1 model. Nonlinear effects on the skewness are discussed in detail in Van Waerbeke et al. (2000b). It should be noted that nonlinear growth of the density field enhances the skewness significantly at scales below 1 degree, so SC correction term remains relatively small because of cancellations between the numerator and the denominator in equation (6). As a consequence, R decreases significantly when  $\theta < 20$ -30 arcmin. It should be also noted that for  $\theta \gtrsim 100$  arcmin, where nonlinear effects can be safely neglected, SC effect is reduced while  $\theta$  increases. This is due to the change in the slope of the density power spectrum occurring when the spatial smoothing scale is of order of the lens position,  $f(\chi)\theta$ .

Let us now discuss the theoretical predictions that take into account nonlinear effects. Figure 4 shows  $S_3$  and R for three cosmologies (top panel) and three bias evolution models (bottom panel). The top panel clearly suggests that it is essential to take SC effect into account to put constraints on values of  $\Omega_{\rm m}$  determined from  $S_3$ . It is also suggested by Figure 4 that SC effect is more important for low than for high density models. This is explained by the fact that the efficiency function is larger in the first than in the second case, as illustrated by Figure 2. Bottom panel of Figure 4 shows as well that SC effect increases with strength of evo-

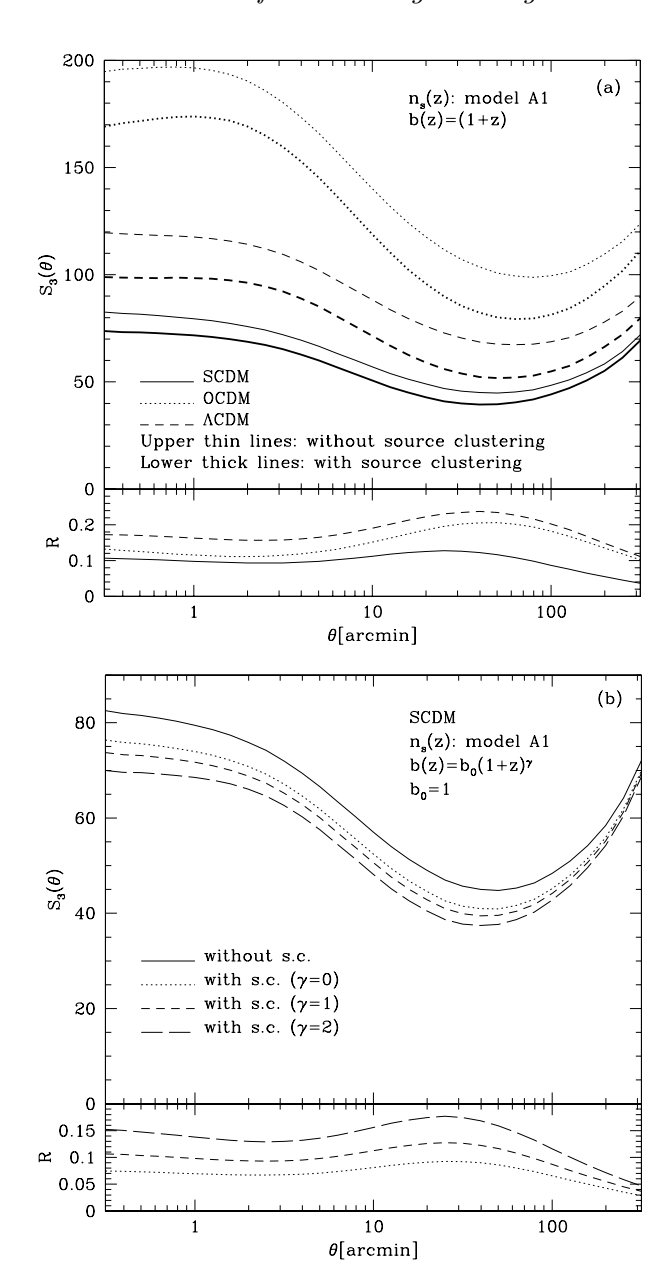
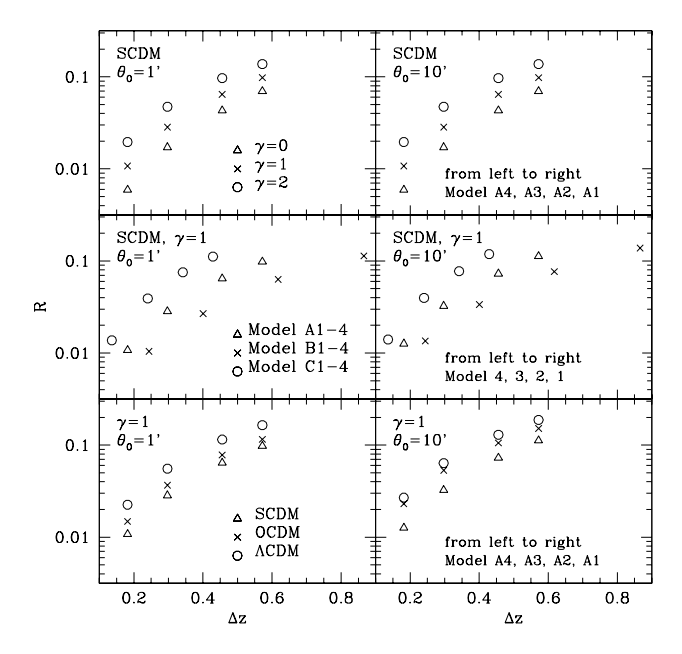


Figure 4.  $S_3$  and R [equation (12)] with and without the source clustering effect taken into account as functions of scale. The nonlinear ansatz is used. Cosmology and source distribution models are denoted in each plot: (a) three different cosmological models are considered; (b) three different bias evolution models are considered.

lution in bias with redshift. This is a natural consequence of the fact that SC effect is caused by the correlation between the lensing potential (the matter distribution) and the distribution of source galaxies. Finally, note that for  $\theta \lesssim 10$  arcmins, relative SC effect is nearly independent of scale.

Figures 3 and 4 show that the relative SC effect, R, presents a peak around  $\theta = 30\text{-}60$  arcmin. One might wonder what should be the ideal smoothing scale for measuring the skewness while reducing as much as possible the SC effect: should it be larger or smaller than the peak position? To answer properly this question, one has to consider as well



**Figure 5.** R as a function of  $\Delta z$  as predicted from our semi-analytic model. The smoothing scales are 1 arcmin and 10 arcmin for left and right panels, respectively. Top panels are for three bias models in SCDM, A1-4, middle panels are for all 12 source distribution models in SCDM  $\gamma=1$  case, and bottom panels are for three cosmological models in  $\gamma=1$  A1-4 cases.

signal-to-noise ratio, S/N. Typically, signal-to-noise in  $S_3$  is expected to decrease with  $\theta$  due to the finiteness of the area covered by the survey. Van Waerbeke, Bernardeau & Mellier (1999) numerically investigated the efficiency of weak lensing surveys, taking both this effect into account and the noise due to intrinsic ellipticity of source galaxies. Figure 8 and 10 of their paper indicate that it might be difficult to detect the skewness with S/N>1 at smoothing scales larger then 60 arcmin, even with a wide field survey covering  $10\times 10$  degree<sup>2</sup>. This suggests that the best choice for the smoothing scale, keeping both SC effects low and a good signal-to-noise ratio, should be  $\theta$  of order of 1 arcmin. †

Figure 5 shows R for  $\theta=1$  arcmin (left panels) and 10 arcmin (right panels) as a function of the source redshift distribution width,  $\Delta z$ . Comparison of left and right panels confirms visual inspection of Fig. 4, namely that R is fairly insensitive to  $\theta$  in the scaling regime considered,  $\theta\lesssim 10$  arcmin. Top and bottom panels indicate that effects of cosmology and bias evolution model on the amplitude of parameter R are significant, but the shape of R as a function of  $\Delta z$  remains fairly stable. Note furthermore that in the middle panels, models with the same mean source redshift form sequences in R- $\Delta z$  plane with very similar slopes at fixed  $\Delta z$ .

This suggests that for a choice of the cosmological model and  $\gamma$ , there exists a simple phenomenological law that relates R to  $\langle z \rangle$  and  $\Delta z$  which is valid for all source models

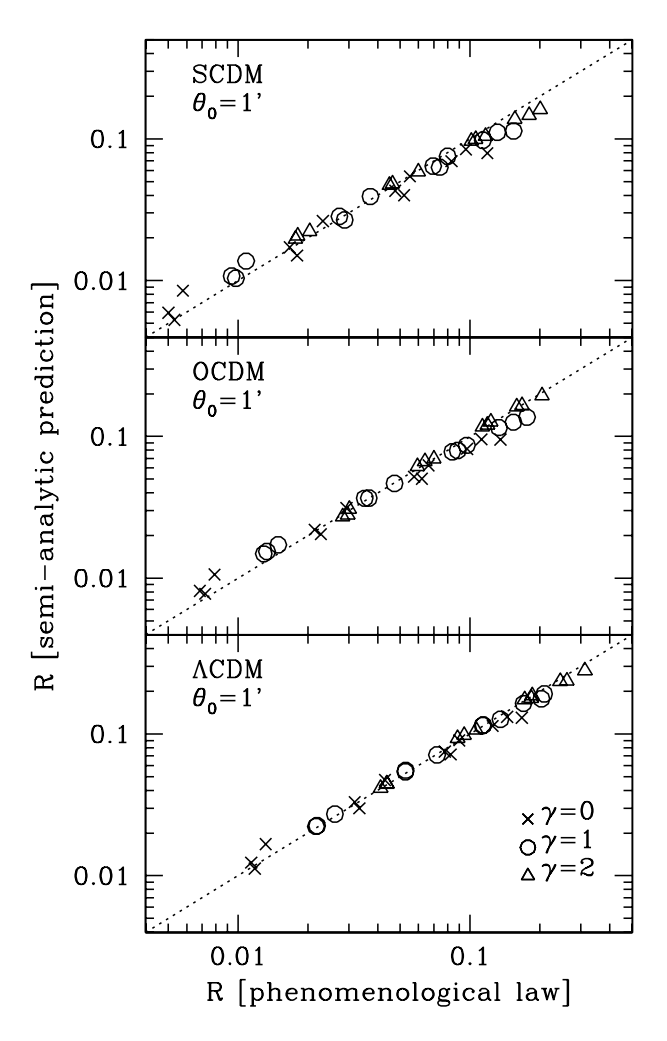


**Figure 6.** R computed by the semi-analytic formula versus that derived from the phenomenological law (Eq. [13]). The parameters (A,B,C) for each case are summarized in Table 3.

**Table 3.** Parameters of the phenomenological law (Eq. [13]) derived from semi-analytic calculations

-		$\theta = 1'$			$\theta = 10'$		
	$\gamma$	A	B	C	A	B	C
SCDM	$\gamma = 0$	0.56	3.0	2.5	0.58	2.9	2.4
	$\gamma = 1$	0.62	2.7	2.2	0.64	2.6	2.1
	$\gamma = 2$	0.70	2.4	1.9	0.72	2.3	1.8
OCDM	$\gamma = 0$	0.59	2.8	2.3	0.43	2.1	1.8
	$\gamma = 1$	0.66	2.5	2.0	0.72	2.3	1.8
	$\gamma = 2$	0.50	1.7	1.5	0.80	2.1	1.6
$\Lambda { m CDM}$	$\gamma = 0$	0.65	2.6	2.1	0.67	2.5	2.0
	$\gamma = 1$	0.72	2.4	1.8	0.75	2.2	1.7
	$\gamma = 2$	0.81	1.8	1.6	0.84	1.9	1.4

considered here,

$$R = A \frac{\Delta z^C}{\langle z \rangle^B},\tag{13}$$

where A is of the order of 0.5, B and C varying from 1.5 to

<sup>&</sup>lt;sup>†</sup> It should be however noted that to break the degeneracy between cosmological parameters, one still has to measure cosmic shear statistics at linear scales, i.e.  $\theta > 1$  degree (Jain & Seljak 1997).

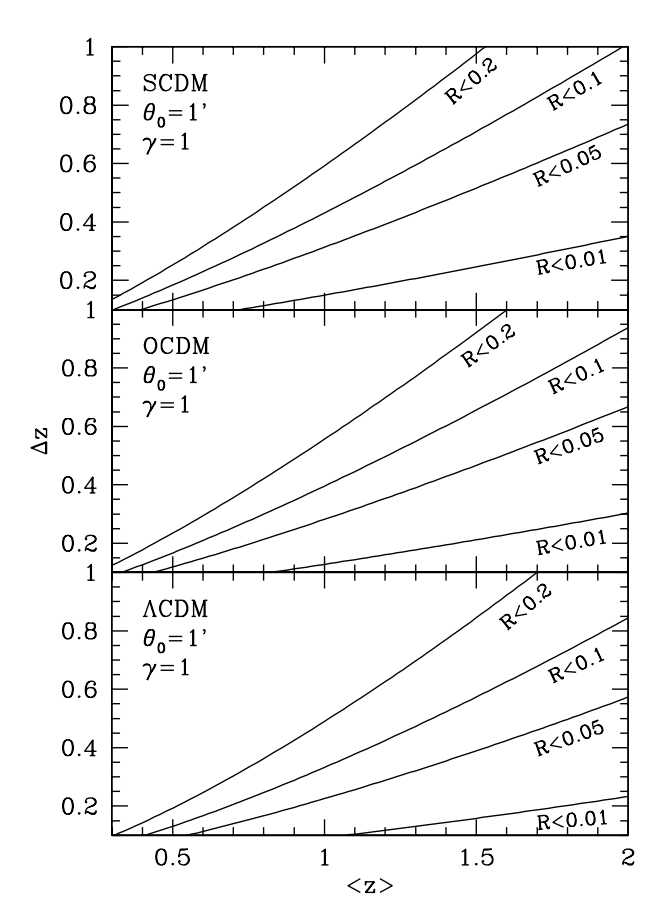


**Figure 7.** Contour lines of R obtained from our semi-analytic modeling in  $\langle z \rangle$ - $\Delta z$  plane for  $\theta = 1'$  and  $\gamma = 1$ . Each panel corresponds to a different cosmology.

3. The precise values parameters (A, B, C) are obtained by a least-square fitting method. They are given in Table 3.

The accuracy of this law is demonstrated in Figure 6. One can see that the data lie fairly well on the parameterized line. It allows us to make a contour plot of parameter R in  $\langle z \rangle$ - $\Delta z$  space, as shown in Fig. 7 for three cosmological models. Not surprisingly, this figure clearly indicates that the way out to reduce SC effect on a measurement of the skewness is to make the source distribution narrow with a high mean redshift.

Finally, we examine the dependence of SC effect on the evolution of bias. Figure 8 shows R's as a function of  $\gamma$  for 4 models selected arbitrarily. For each source distribution model, the R- $\gamma$  relation is well fitted by the following empirical law,

$$\log R = \epsilon \gamma + \text{const} \,. \tag{14}$$

Coefficient  $\epsilon$  is shown in Fig. 9 as a function of  $R(\gamma=1)$  for all source distribution models we consider. Each panel corresponds to a given choice of cosmology. One can see that  $\epsilon$  remains in the range  $0.1 < \epsilon < 0.3$  and is almost insensitive to both smoothing scale and cosmology. At fixed value of  $R(\gamma=1)$ ,  $\epsilon$  increases with mean redshift (in order of C, A and B). Indeed, for our choice of function b(z), the impact of bias evolution is more significant at higher redshift.

The uncertainty in parameter R caused by our ignorance of b(z) can be roughly estimated using the empirical

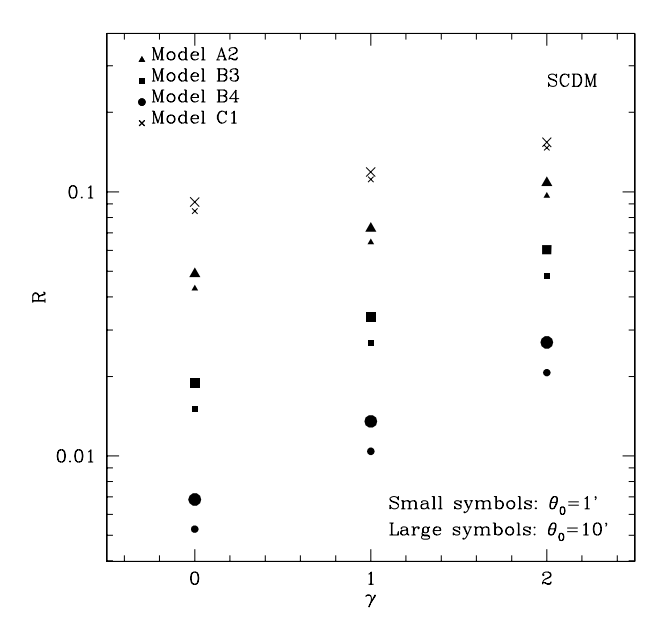
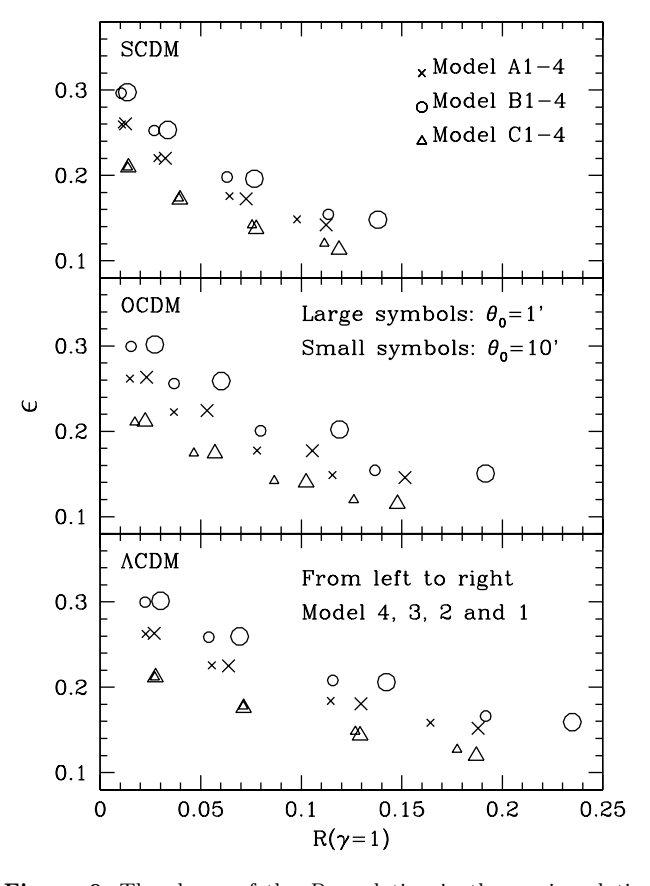


Figure 8. semi-analytic values of R's as a function of  $\gamma$  for 4 selected models in SCDM.



**Figure 9.** The slopes of the R- $\gamma$  relation in the semi-analytic model. Coefficient  $\epsilon$  as defined in equation (14) is shown as a function of  $R(\gamma = 1)$ .

relation (14) as follows: suppose that the power-law model (11) for the evolution of bias stands, but that there is an error  $\Delta_{\gamma}$  on the value of  $\gamma$ . Applying simple error propagation technique, one finds  $\delta R/R=2.3\,\epsilon\,\Delta_{\gamma}(\sim\,0.5\Delta_{\gamma})$ : if one is able to constrain the bias evolution model with an accuracy better than  $\Delta_{\gamma}<0.4$ , the uncertainty in R drops below 20 percent.

# 6 TESTING SEMI-ANALYTIC PREDICTIONS AGAINST NUMERICAL SIMULATIONS

In this section, we compare theoretical predictions to ray-tracing experiments in N-body simulations, using mock galaxy catalogs extracted from the simulations as distributions of sources. The N-body data sets and the ray-tracing method used for this work are described in  $\S$  6.1.  $\S$  6.2 details the procedure used to generate mock galaxy catalogs. Finally,  $\S$  6.3 presents the results of the comparison. We focus only on SCDM model, but the conclusions of our numerical analysis should not depend significantly on the considered cosmology.

# 6.1 A brief description of the ray-tracing simulations

Light ray trajectories are followed through large N-body simulations data set generated with a fully vectorized and parallelized Particle-Mesh (PM) code (e.g., Colombi, Devriendt & Szapudi, 2000). This PM code has been inspired by original works of Bouchet, Adam & Pellat (1985), Alimi et al. (1990) Moutarde et al. (1991) and Hivon (1995). Each N-body experiment involves  $256^2 \times 512$  particles in a periodic rectangular box of size (L, L, 2L). The mesh used to compute the forces was  $256^2 \times 512$ . A light-cone of the particles was extracted from each simulation during the run as explained in Hamana, Colombi & Suto (2000a, see also Colombi et al. 2000 for more technical details). Our aim was the light-cone to cover a large redshift range,  $0 \le z \le 3$ , and a field of view of  $5 \times 5$  square degrees. To do that, we adopted the tiling technique first proposed by White & Hu (2000): we performed 11 independent simulations covering adjacent redshift intervals  $[z_i^{\min}, z_i^{\max}], i = 1, \dots, 11$ . The size of each simulation is such that the portion of the lightcone in  $[z_i^{\min}, z_i^{\max}]$  (aligned with the third axis) exactly fits the box-size. This way, angular resolution is approximately conserved as a function of redshift, except close to the observer. Finally, in order to have enough structures in each box, we impose the supplementary constraint  $L \geq 80h^{-1}$ Mpc. As a result, L follows the following sequence with redshift, 80, 80, 80, 80, 80, 120, 160, 240, 320, 480, 640  $h^{-1}$  Mpc. More details and technical discussions on this procedure will be found in Hamana, Colombi & Mellier 2000b.

The multiple lens-plane algorithm was used for ray-tracing calculations (Jain et al. 2000 and references therein). The lens planes (which are, at the same time, source planes) are separated by intervals of  $80h^{-1}{\rm Mpc}$ , amounting to a total number of 38 in the redshift range  $0 \le z \le 3$ . For each ray, the lensing magnification matrix is computed on the source planes and is stored. We performed 40 realizations of the underlying density field by random shifts of the simulation boxes in the (x, y) plane. For each realization,  $512^2$ 

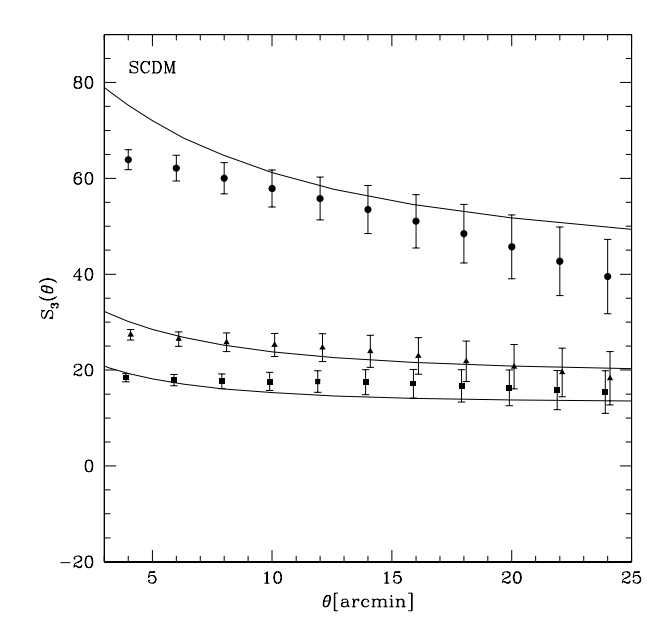


Figure 10. The skewness  $S_3$  of the lensing convergence measured from the ray-tracing simulations (symbols) compared with nonlinear predictions (solid lines) for single source redshifts  $z_s \sim 1$  (top), 2, and 3 (bottom).

rays are traced backward from the observer. The initial ray directions are set on  $512^2$  grids, which correspond to pixels of angular size  $5^\circ/512 \sim 0.59$  arcmin.

Before using realistic redshift distribution of sources, we compute the skewness of the lensing convergence for single source planes, i.e.,  $n_s(z) = \delta_D(z=z_s)$  where  $\delta_D$  is the Dirac's delta function. At this stage, we do not take into account SC effect yet. Figure 10 shows  $S_3$  obtained from the simulations compared to nonlinear predictions. Measurements match theory reasonably well, as expected (Van Waerbeke et al. 2000b). There are slight differences which can be explained as follows:

- (i) The N-body simulations have a finite spatial resolution, which implies a flattening of  $S_3$  at scales smaller than about 4 arcmin.
- (ii) At large angular scales,  $\theta \gtrsim 20-30$  arcmin, depending on the source redshift considered (Hamana et al. 2000), the measured  $S_3$  underestimates the real value, due to finite volume effects (i.e. due to the finite size of the simulation boxes, e.g., Colombi, Bouchet & Schaeffer 1994).
- (iii) There is an uncertainty in the fitting formula of the density bispectrum (section 3), which transforms into a 10-20 percent error on the semi-analytic prediction for  $S_3$ . The differences between theory and measurements in Fig. 10 are not larger than this expectation, at least in the available dynamic range,  $4 \lesssim \theta \lesssim 20-30$  arcmin (derived from the above discussion on spatial resolution and finite volume effects).

In conclusion, without SC effects (yet) taken into account, the semi-analytic prediction obtained for  $S_3$  is accurate (Van Waerbeke et al. 2000b).

#### 6.2 Mock galaxy catalogs

We generated three mock galaxy catalogs with realistic galaxy number counts  $n_{\rm s}(z)$  and reproducing as well as possible the power-law model for function b(z),  $b(z)=(1+z)^{\gamma}$  with  $\gamma=0,\,1,\,$  and 2. They are extracted exactly from the same dark matter distributions as the ones used for the raytracing simulations.

The procedure to create the mock catalogs (Stebbins 1995; Colombi et al. 2000) can be described as follows:

(i) We adopt threshold biasing, i.e. for a smooth density distribution of dark matter, we assume that galaxies lie in regions of density contrast larger than some threshold which may eventually depend on redshift [point (ii) below],  $\delta \geq \delta_{\rm TH}(z)$ . Inside these regions, the local number density of galaxies at position  $(z,\theta,\phi)$ , is proportional to dark matter density

$$n_{\mathbf{g}}(z,\theta,\phi) = \mu(z)[1 + \delta(z,\theta,\phi)]. \tag{15}$$

The normalization factor  $\mu(z)$  is such that the redshift distribution of galaxies reproduces (in terms of ensemble average) some prior,  $n_{\rm s}(z)$ , discussed in (iii). To estimate the local density contrast from our discrete dark-matter particle distribution, we use local adaptive smoothing: the mean quadratic distance d between each simulation particle and its 6 nearest neighbors is computed. Then,  $1 + \delta \propto d^{-3}$ . For each dark matter particle in regions with  $\delta > \delta_{\rm TH}$ , N galaxies are randomly placed in the sphere of radius d centered on the particle position. N is computed from a random realization of a Poisson distribution with average  $\bar{N} = (4/3)\pi d^3 n_{\rm g}$ .

(ii) Function  $\delta_{\text{TH}}(z)$  is determined numerically so that the measured variances of density fluctuations in a sphere of radius  $8h^{-1}$  Mpc in the galaxy and the dark matter distribution, respectively  $\sigma_8^{\text{gal}}$  and  $\sigma_8$ , verify

$$\frac{\sigma_8^{\text{gal.}}(z)}{\sigma_8(z)} = b(z). \tag{16}$$

To do that, we use snapshots of the simulations at various redshifts  $z_i$ , and compute iteratively  $\delta_{\rm TH}(z_i)$  to match equation (16) within a 3 percent accuracy. Then function  $\delta_{\rm TH}(z)$  is obtained by linear interpolation of the  $\delta_{\rm TH}(z_i)$ . Note that for  $\gamma=0$ , we simply have  $\delta_{\rm TH}=-1$ .

(iii) A prior function  $n_s(z)$  is needed to compute the normalization factor  $\mu(z)$  equation (15). We have used the ab-initio semi-analytic approach to galaxy formation described in Devriendt & Guiderdoni (2000) to obtain a reasonably realistic estimate of this function. Such an approach is based on a Press-Schechter like prescription to compute the number of galaxies as a function of redshift, coupled to spectro-photometric evolution of stellar populations to calculate their luminosities. The results naturally match observed galaxy number counts and redshift distributions, as well as the diffuse extragalactic background light for wavelengths ranging from the UV to the near IR. Here, we suppose that galaxies are selected in the I band, down to the magnitude  $I_{AB} = 24.5$ . As a result, the final mock catalogs yields a typical surface number density of 29 sources per arcmin<sup>2</sup> distributed in redshift as shown in Figure 11. The distribution has a peak at  $z \sim 0.4$ , with mean redshift  $\langle z \rangle \sim 0.8$  and typical width  $\Delta z \sim 0.6$ .

More technical details on the procedure used to generate

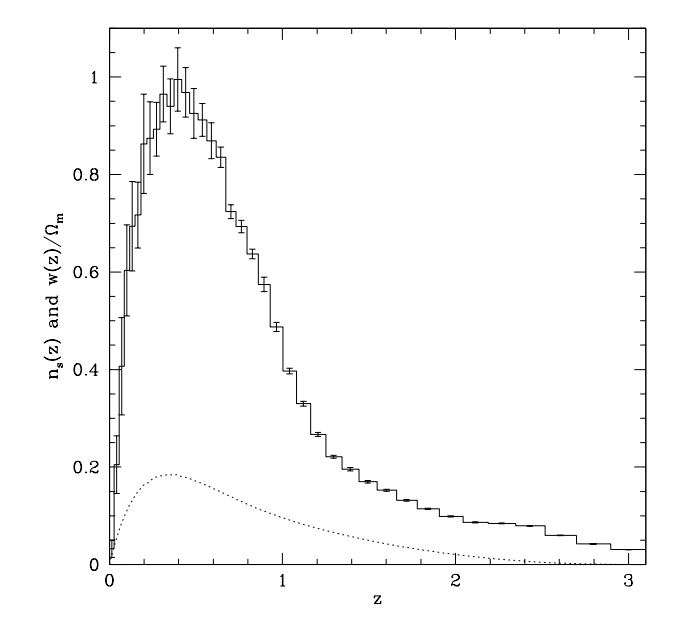


**Figure 11.** The distribution of sources (histogram with error bars) and the lensing efficiency function (dotted line) as functions of redshift. Error bars denote standard deviation computed among 40 realizations as discussed in Sect. 6.1.

mock catalogs will be found in Colombi et al. (2000). Note that instead of using threshold bias, we could simply have taken pure linear bias exactly as assumed in the theoretical calculations. However, we think that threshold bias is more realistic. Moreover, to test the robustness of semi-analytic predictions, it is interesting to use a slightly different biasing prescription for the numerical experiments.

Figures 12, 13 and 14 give a visual impression of the mock catalogs for 3 values of  $\gamma$ . As expected, clumpiness augments with  $\gamma$ . It is tempting to conclude that the most realistic catalog corresponds to  $\gamma=1$ . In the unbiased case, there are no voids, whereas in the  $\gamma=2$  case, the simulated galaxy distribution is so clumpy that it looks like a Rayleigh-Lévy random walk, especially at high redshift.

Figure 15 shows the scaling behavior of the bias factor defined by

$$\tilde{b}(z,\ell) \equiv \frac{\sigma_{\text{gal.}}(\ell)}{\sigma}(\ell),\tag{17}$$

as measured in the mock catalogs with  $\gamma=1$  and  $\gamma=2$ . In this equation,  $\sigma_{\rm gal.}^2(\ell)$  and  $\sigma^2(\ell)$  are respectively the variances in a sphere of radius  $\ell$  of the galaxy and the matter density distribution. In fact, we take for  $\sigma^2$  the variance measured in the mock catalog with  $\gamma=0$  which is unbiased by definition. To correct for variations of the selection function we use the method proposed by Colombi, Szapudi & Szalay (1998). The curves on each panel correspond to redshift slices of [0.16,0.20], [0.3,0.36], [0.56,0.68], [1.09,1.41] and [2.40,3.00].

By construction, the value of  $\tilde{b}$  measured at  $\ell=8^{-1}{\rm Mpc}$  (triangles) matches very well relation (16). However there is no guarantee for this result to hold at all scales. In other words, at fixed z, function  $\tilde{b}(\ell,z)$  is not necessarily a constant of scale [and equal to  $b(z)=(1+z)^{\gamma}$ ], although this is pretty much the case for the  $\gamma=1$  mock catalog.

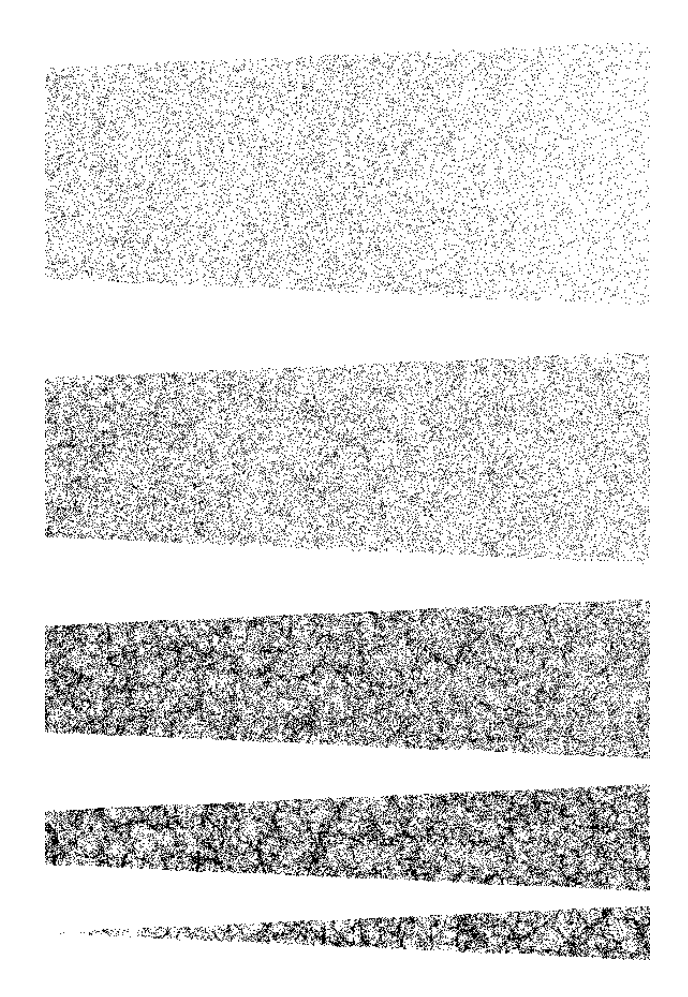
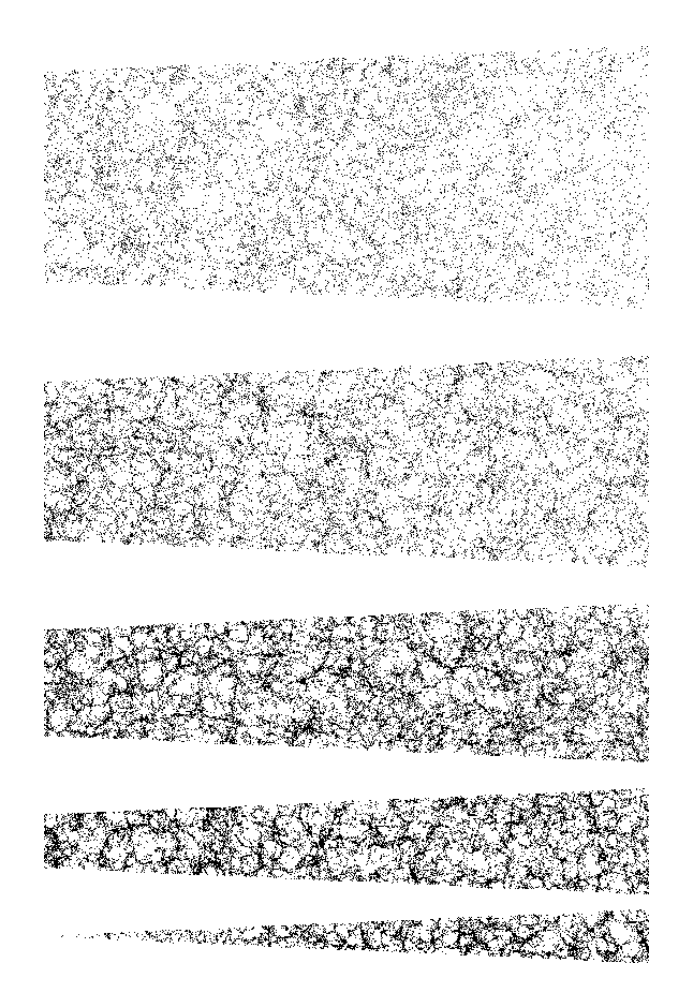


Figure 12. Sketch of the mock catalog in the  $\gamma=0$  case. The part of the light cone which is represented covers  $5\times0.5$  degree<sup>2</sup>. The observer is at the lower-left corner, and distance from the observer increases from left to right and from bottom to top. Each point corresponds to a galaxy and is displayed in comoving coordinates space, up to  $z\simeq3.1$ .

For the  $\gamma=2$  mock catalog, function  $b(\ell,z)$  presents large variations with scale, increasingly with redshift. This can be modeled as a varying effective  $\tilde{\gamma}(\ell)$ , for example  $\tilde{\gamma}\simeq 3$  for  $\ell=1h^{-1}$  Mpc (squares on bottom panel of Fig. 15). While converting scales to angles, more relevant to our analysis, the modeling in terms of a function  $\tilde{\gamma}(\theta)$  is not very convincing. Still, we find that in the range of interest,  $4\lesssim\theta\lesssim20-30$  arcmin, we should compare measured SC effects to semi-analytic predictions corresponding to  $2\lesssim\gamma\lesssim3$ .

### 6.3 Results

We measure convergence statistics on mock galaxy catalogs as follows: the value of convergence for a galaxy at redshift z is given by linear interpolation between the  $\kappa_i$  –computed from rays propagating between redshift z of the closest lens plane to the galaxy (see § 6.1) and present time—measured at the four nearest angular pixels from the galaxy position in the sky. The amplitude of SC effect is measured by comparing simulations to similar SC-free ones. They are obtained



**Figure 13.** Same as in Fig. 12, but for  $\gamma = 1$ .

from other mock galaxy catalogs with the same source distribution  $n_s(z)$  (i.e. the same as in the SC mock catalog), in which galaxies are randomly distributed on the sky. Note finally that top hat filtering is used and intrinsic ellipticity of galaxies is not taken into account.

Upper panel of Fig. 16 shows the skewness parameter measured from the  $\gamma = 1$  mock galaxy catalog with and without SC effect. Lower panel displays function  $R(\theta)$ , except that in the denominator of equation (12), we always take the value given by nonlinear semi-analytic predictions,  $S_3^{n.l.}$ . As discussed in § 6.1, the simulations have limited available dynamic range since they are contaminated by force softening and finite volume effects respectively at small and large scales, where the measured  $S_3$  is expected to underestimate the real value. Furthermore, there is a 10-20 percent uncertainty on nonlinear perturbation theory predictions. With these elements in mind, we see that agreement between measurements and predictions is still very good when SC effect are taken into account. In particular, the order of magnitude of the shift between the upper and the lower symbols in top panel of Fig. 16 matches very well that between the dotted and the solid curve, as illustrated by bottom panel.

Similar results are obtained for the  $\gamma=0$  and 2 catalogs, as summarized in Fig. 17, which concentrates on the param-

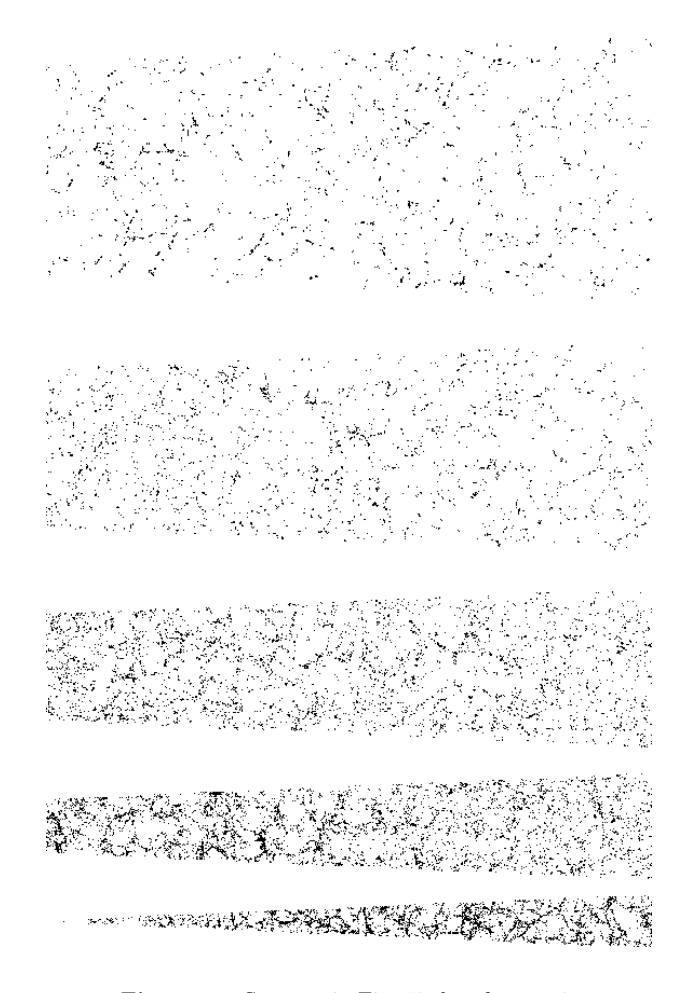


**Figure 14.** Same as in Fig. 12, but for  $\gamma = 2$ .

eter R. Detailed examinations reveal a systematic shift between theory and measurements, particularly significant for the  $\gamma=2$  catalog. This slight disagreement is not surprising since (i) numerical experiments are done with threshold bias instead of simple linear bias, (ii) theoretical calculations do not take into account intrinsic clustering of source galaxies as discussed in last paragraph of § 2. In fact, the match between measurements and predictions is amazingly good, especially given point (i), but not perfect, in particular for the  $\gamma=2$  catalog. This latter agrees better with theoretical predictions for  $\gamma=3$  than for  $\gamma=2$ , except at the largest angular scales. However, this is actually in good agreement with results of § 6.2, where the measured bias between galaxies and dark matter was showing a strong scale dependence corresponding to effective values of  $\gamma$  between 2 and 3.

#### 7 SUMMARY AND DISCUSSION

We have examined source clustering (SC) effect on measurements of the skewness of lensing convergence using a non-linear semi-analytic approach. The result of semi-analytic predictions were tested against numerical simulations, and a good agreement between them was found. Our main conclusions are as follows:

• SC effect strongly depends on the redshift distribution

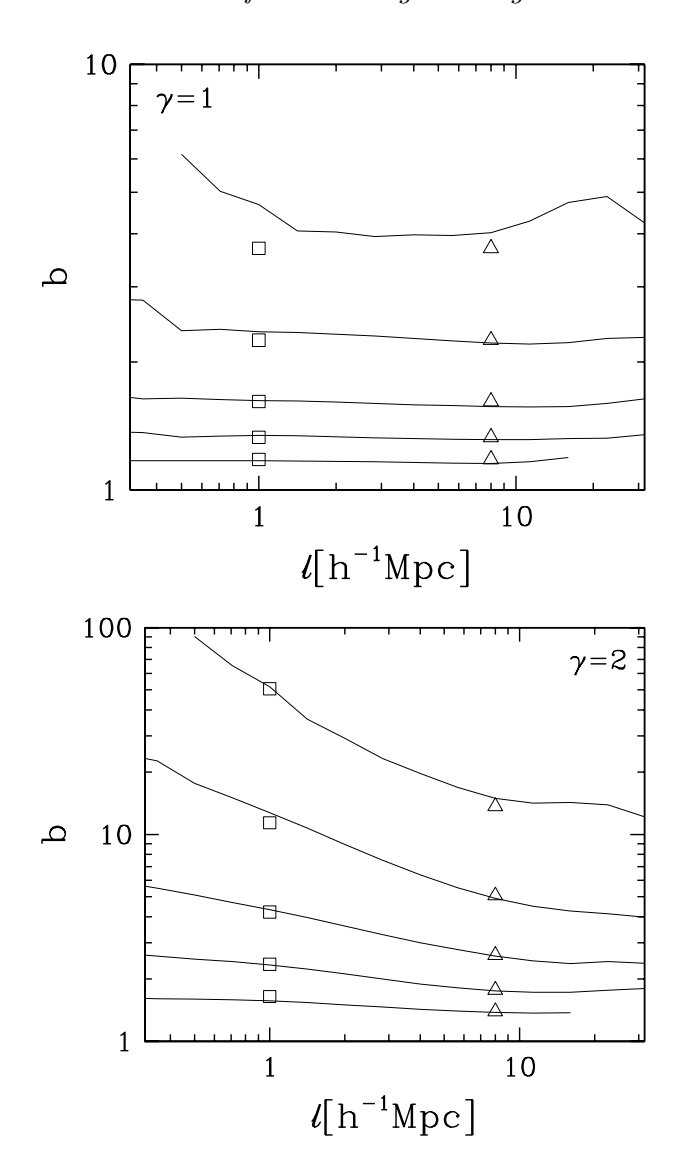


Figure 15. The biasing function  $\tilde{b}$  [equation (17)] as a function of spatial scale  $\ell$ , measured in the mock galaxy catalogs. The top and bottom panels correspond respectively to  $\gamma=1$  and  $\gamma=2$  (by construction, we exactly have  $\tilde{b}=1$  for  $\gamma=0$ ). Each curve is for a fixed value of z, namely  $z\simeq 0.18, 0.33, 0.62, 1.25$  and 2.70 from bottom to top of each panel. On the top panel, the squares and the triangle give the values expected from b(z)=1+z. On the bottom panel, the square and the triangle correspond respectively to  $b(z)=(1+z)^3$  and  $b(z)=(1+z)^2$ .

of source galaxies. We found that the effect scales with the width and mean redshift of the distribution roughly as  $R \propto \langle z \rangle^{-(3.0-1.8)} \Delta z^{1.4-2.5}$ , (where  $R = -S_3^{s.c.}/S_3$ , and  $S_3^{s.c.}$  is the change in measured  $S_3$  due to SC). As illustrated by Fig. 7, this relation indicates that it is essential to make the width of the distribution narrow and to make the mean redshift high for reducing SC effect (this was partly pointed out by B98).

• SC effect also depends on evolution of the bias between the galaxy and the total matter distribution, b(z). Assuming a simple power-law model,  $b(z) \propto (1+z)^{\gamma}$ , we found that the uncertainty in  $\gamma$  transforms into  $\delta R/R = 2.3 \epsilon \Delta_{\gamma}$  with a

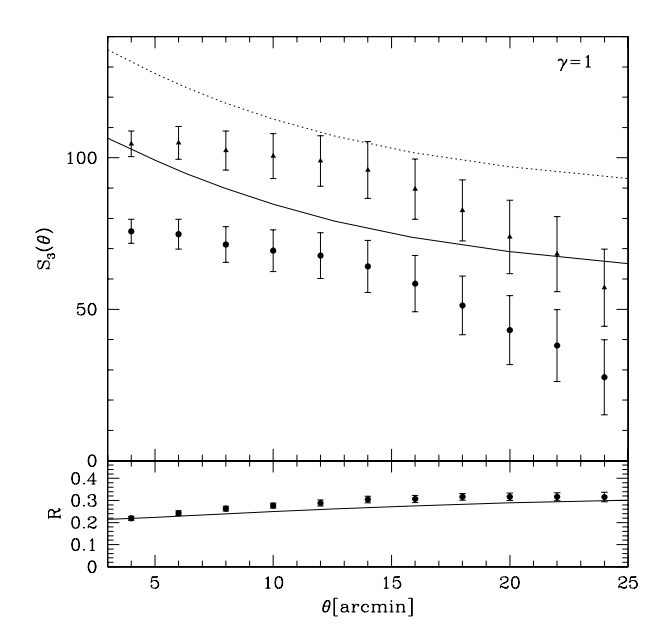


Figure 16.  $S_3$  (upper panel) and R (lower panel) as functions of the smoothing angle  $\theta$  in the  $\gamma=1$  case. Symbols and curves denote results of ray-tracing simulations and semi-analytic predictions respectively. Error bars give some estimate of the uncertainty E on the measurements, i.e.  $E(S_3) \simeq \Delta S_3/\sqrt{40}$ , where  $(\Delta S_3)^2$  is the dispersion over the 40 realizations. Note that R is calculated as  $R=-S_3^{s.c.}/S_3^{n.l.}$ , where  $S_3^{n.l.}$  is always given by semi-analytic predictions.

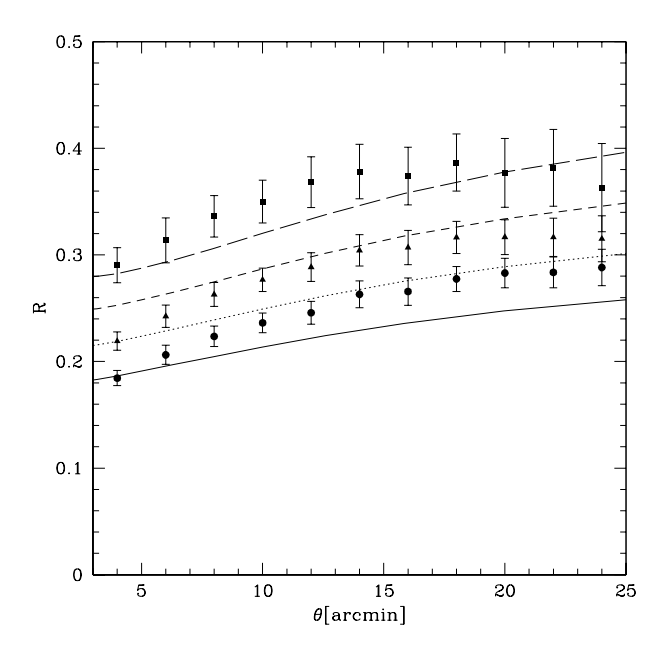


Figure 17. The parameter R as displayed in lower panel of Fig. 16 but now for all values of  $\gamma$  considered. Symbols shows the results of ray-tracing simulations: Circles, triangles and squares correspond respectively to  $\gamma=0,\,1$  and 2 mock catalogs. Lines correspond to semi-analytical prediction,  $\gamma=0,\,1,\,2,\,3$  from bottom to top. Error bars are computed as explained in caption of Fig. 16.

typical value of  $\epsilon \sim 0.2$ . This indicates that the uncertainty in  $\gamma$  must be  $\Delta_{\gamma} < 0.2$  for predicting the amplitude of the SC effect within better than 10 percent accuracy.

The main uncertainty in semi-analytic predictions comes from the fact that the nonlinear fitting formula of the density bispectrum is only 10-20 percent accurate. We expect the same level of uncertainty in predictions presented in this paper for the SC effect on the skewness. This can actually be improved by measurements in large N-body simulations with high spatial resolution.

Since, so far, little is known about the evolution of the bias, it is still very difficult to predict SC effect accurately. It is therefore very important to reduce this latter as much as possible by controlling the redshift distribution of sources. It follows from the above results that an ideal observational strategy might be as follows: (i) going to a deep limiting magnitude to increase mean redshift survey and (ii) using only fainter images to reduce the width of the distribution. A desirable source distribution for R < 0.1 suggested by Fig. 7 would have  $\Delta z < 0.3$  and  $\langle z \rangle > 1$ . This may be of course challenging: going to deeper magnitudes will make the calculation of the redshift distribution of sources more difficult and using only faint images will increase the noise due to intrinsic ellipticity in galaxies. We leave more detailed studies on the designing of optimal strategies to future works.

# ACKNOWLEDGMENTS

We would like to thank L. Van Waerbeke for providing the FORTRAN code to compute the nonlinear skewness of convergence and for helpful comments. We would also like to thank A. Stebbins for teaching us his way of generating mock galaxy catalogs from N-body simulations. This research was supported in part by the Direction de la Recherche du Ministère Français de la Recherche. The computational means (CRAY-98) to do the N-body simulations were made available to us thanks to the scientific council of the Institut du Développement et des Ressources en Informatique Scientifique (IDRIS). Numerical computation in this work was partly carried out at IAP at the the TERAPIX data center and on MAGIQUE (SGI-02K).

# REFERENCES

Alimi J.-M., Bouchet F. R., Pellat R., Sygnet J.-F., Moutarde F., 1990, ApJ, 354, 3

 Bacon D., Refregier A., Ellis. R., 2000, MNRAS, 318, 625
 Bartelmann M., Schneider P., 2000, to be appeared in Physics Report, (astro-ph/9912508)

Bernardeau F., 1998, A&A, 338, 375 (B98)

Bernardeau F., Van Waerbeke L., Mellier Y., 1997, A&A, 322, 1 (BvWM97)

Bond J. R., Efstathiou, G., 1984, ApJ, 285, L45

Bouchet F. R., Adam J.-C., Pellat R., 1985, A&A, 144, 413

Colombi S., Bouchet F. R., Schaeffer R., 1994, A&A, 281, 301

Colombi S. T., Devriendt J. E. G. T., Szapudi, I., 2000, in preparation

Colombi S., Szapudi I., Szalay A.S., 1998, MNRAS, 296, 253
Devriendt J. E. G., Guiderdoni B., 2000, A&A, 363, 851
Eke V. R., Cole S., Frenk C. S., 1996, MNRAS, 282, 263
Hamana T., Colombi S., Suto Y., 2000a, A&A in press (astro-ph/0019287)

Hamana T., Colombi S. T., Mellier Y., 2000b, in preparation

Hivon E., 1995, Ph.D. thesis, Université Paris XI

Jain B., Seljak U., 1997, ApJ, 484, 560

Jain B., Seljak U., White S. D. M., 2000, ApJ, 530, 547

Jenkins A., et al. (The Virgo consortium), 1997, ApJ, 499, 20

Kaiser N., 1992, ApJ, 388, 272

Kaiser N., 1998, ApJ, 498, 26

Kaiser N., Wilson G., Luppino G. A., 2000, ApJ submitted (astro-ph/0003338)

Kitayama T., Suto Y., 1997, ApJ, 490, 557

Maoli R., et al., 2000, A&A submitted (astro-ph/0011251)

Mellier Y., 1999, ARA&A, 37, 127

Moutarde F., Alimi J. M., Bouchet F. R., Pellat R., Ramani A., 1991, ApJ, 382, 377

Peacock J. A., Dodds, S. J., 1996, MNRAS, 280, L19

Peebles P. J. E., 1980, The Large Scale Structure of the Universe, Princeton Univ. Press, Princeton

Schneider P., Van Waerbeke L., Jain B., Kruse G., 1998, MNRAS, 296, 873

Scoccimarro R., Couchman H. M. P., 2000, MNRAS submitted (astro-ph/0009427)

Stebbins A., 1995, private communication

Thion A., Mellier Y., Bernardeau F., Bertin E., Erben T., van Waerbeke L., To appear in the Proceedings of the XXth Moriond Astrophysics Meeting "Cosmological Physics with Gravitational Lensing", eds. J.-P. Kneib, Y. Mellier, M. Moniez and J. Tran Thanh Van

Van Waerbeke L., Bernardeau F., Mellier Y., 1999, A&A, 342, 15

Van Waerbeke L., et al., 2000a, A&A, 358, 30

Van Waerbeke L., Hamana T., Scoccimarro R., Colombi S., Bernardeau F., 2000b, MNRAS, in press (astro-ph/0009426)

White. M., Hu W., 2000, ApJ, 537, 1

Wittman D. N., et al., 2000, Nature, 405, 143

This paper has been produced using the Royal Astronomical Society/Blackwell Science LATEX style file.